ACS APPLIED MATERIALS & INTERFACES

www.acsami.org

Research Article

Enhanced Stability for Nitrate Electrosynthesis by Heterogeneous FeOOH−TiO_2 Anchored on 2-Methylimidazolium Functionalized Polypyrrole/Graphene Oxide

Rui Zhang,*[,⊥] Huinan Li,[⊥] Yuheng Sun, Shuyao Wu, Qiong Wu, Tianyi Ma, Daliang Liu,* and Hui Mao*

Cite This: https://doi.org/10.1021/acsami.5c16699

Read Online

ACCESS | Metrics & More | Article Recommendations | Supporting Information

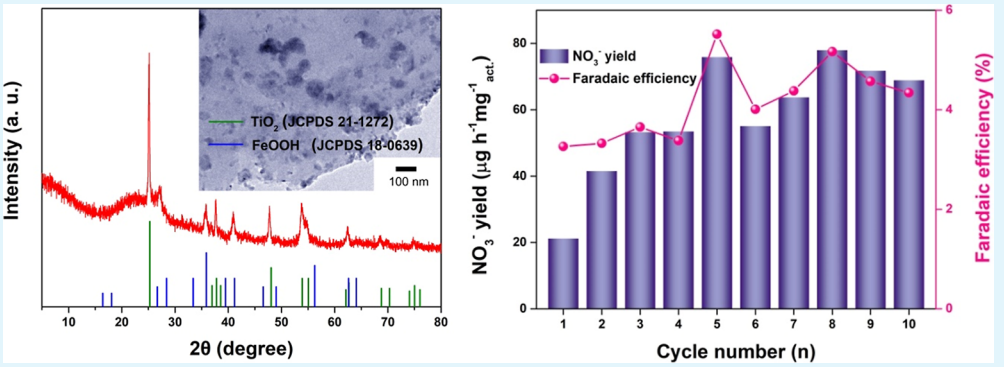

ABSTRACT: The electrocatalytic nitrogen oxidation reaction (NOR) technology offers an environmentally friendly, cost-efficient, and controllable method for nitrate production under mild conditions. Advances in NOR heavily rely on the discovery of effective and affordable electrocatalysts. This study unveils a novel approach by meticulously integrating FeOOH−TiO_2 heterostructures onto a sophisticated substrate of 2-methylimidazolium functionalized polypyrrole/graphene oxide (2-MeIm/PPy/GO), through in situ growth processes involving ion-exchange and coordination between the 2-MeIm groups and metal precursors. The resulting FeOOH−TiO_2@2-MeIm/PPy/GO exhibits remarkable resilience during the NOR process, which achieves a notable NO_3^- yield of 83.24 $\mu g\ h^{-1}\ mg_{act.}^{-1}$, accompanied by a peak Faradaic efficiency (FE) of 5.47% at 1.94 V (vs reversible hydrogen electrode). Nitrogen oxidation primarily occurs at iron sites, where the doped Fe^{2+} in TiO_2 can all gradually convert to Fe^{3+} during the process; meanwhile, titanium sites within FeOOH−TiO_2@2-MeIm/PPy/GO maintain stable chemical states, ensuring sufficient electroactivity for oxygen evolution reactions (OER) to produce *O necessary for nonelectrochemical steps in NOR. This synergistic interplay between iron and titanium contributes significantly to both the stability and durability of FeOOH−TiO_2@2-MeIm/PPy/GO, positioning it as a promising candidate for real-world NOR applications. This work provides valuable insights into the design and fabrication of next-generation electrocatalysts for sustainable nitrate production.

KEYWORDS: *FeOOH, TiO_2, 2-methylimidazolium functionalized polypyrrole/graphene oxide (2-MeIm/PPy/GO), nitrogen oxidation reaction (NOR), enhanced stability*

1. INTRODUCTION

Electrocatalysis offers a promising path toward sustainable chemical processes by utilizing electricity as a clean energy source.[1] This technology enables greener and more efficient manufacturing compared to traditional methods, exemplified by the electrosynthesis of nitrate via nitrogen oxidation reaction (NOR), which surpasses the energy efficiency of the conventional Ostwald process.[2−4] The effectiveness of electrocatalysis for nitrate production heavily relies on the selection and design of the catalyst. While precious metals like platinum exhibit high activity in N_2 activation due to their ability to break the strong N≡N triple bond at low overpotential,[5−7] their scarcity and cost hinder widespread application.[8] Consequently, research has shifted toward nonprecious metal catalysts for electrocatalytic nitrogen fixation, with significant progress made in the field of nitrogen reduction reaction (NRR).[9,10] However, NOR electrocatalysts remain in early stages of development,[11−13] and its large-scale production faces

Received: August 21, 2025
Revised: September 24, 2025
Accepted: October 5, 2025

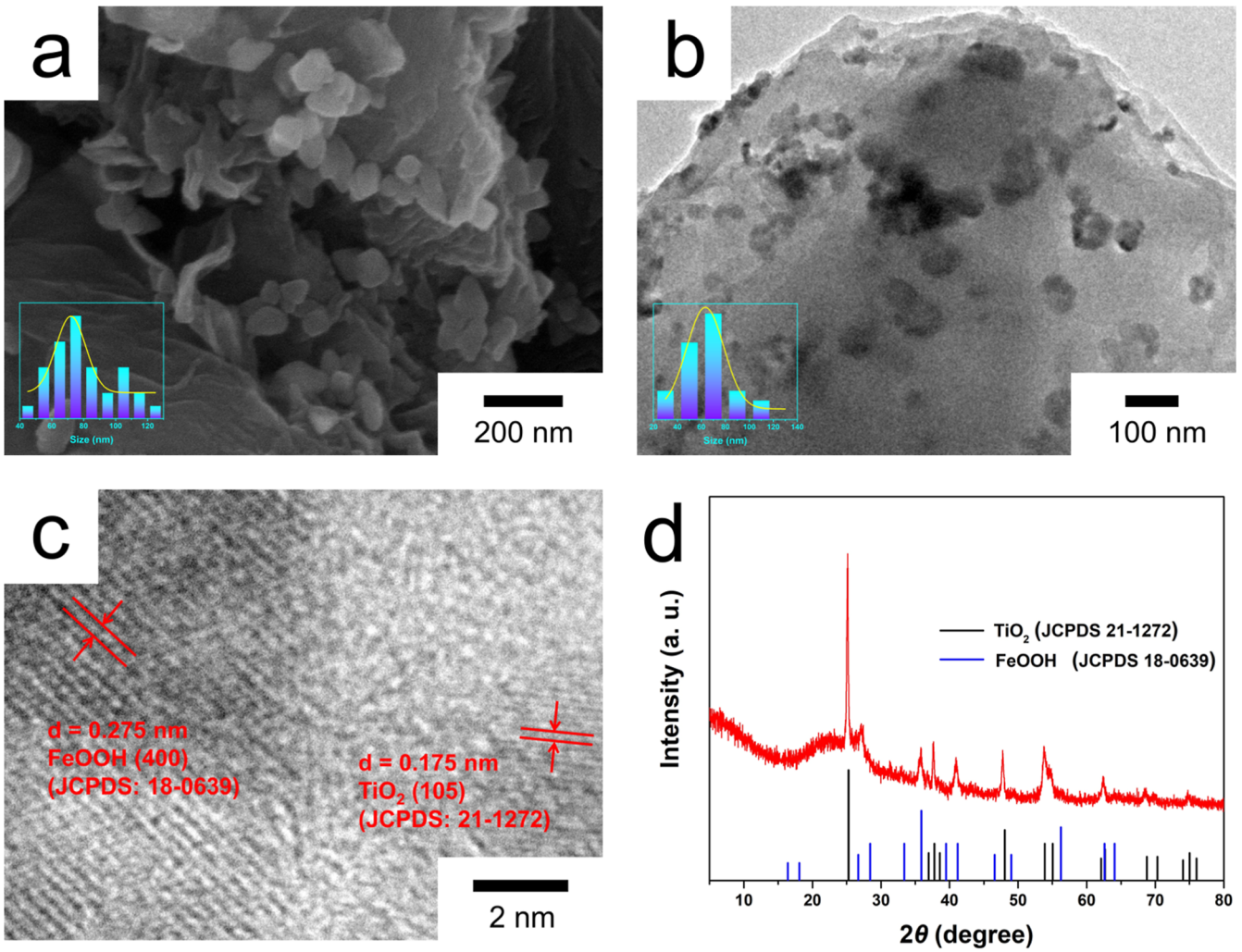

Figure 1. (a) SEM image; (b) TEM image; (c) HRTEM image; (d) XRD pattern of FeOOH−TiO_2@2-MeIm/PPy/GO.

multiple challenges, especially related to density limitations, production scalability, economic feasibility, and environmental impact.[14] For instance, suitable support materials are crucial for catalyst dispersion and activity, but high-density supports may hinder reactant diffusion, reducing reaction rates.[15] Larger catalyst particles may prevent reactants from effectively contacting active sites, diminishing catalytic efficiency.[16] Conversely, very small particles may lack mechanical strength. The synthesis methods for large-scale catalyst production can be complex and costly; meanwhile, ensuring consistent performance and reproducibility of catalysts across batches in large-scale production is challenging. Therefore, the development of efficient NOR electrocatalysts with stable performance and low cost is of vital importance for the practical application of nitrate electrosynthesis.

Both theoretical and experimental studies agree that chemisorption and electron transfer activation of N_2 at the catalytic active site are crucial for N_2 conversion. Nonprecious transition metals (TMs), particularly Fe, Mo, and Ti,[17] demonstrate an affinity for binding N_2 molecules due to their empty and occupied d orbitals.[18] The unoccupied d orbital of TMs can accept the lone pair electrons from N_2, while the occupied d orbitals donate electrons to the empty π^* orbital of N_2.[19] The catalytic activity is often correlated to the binding energy between the metal and nitrogenous substances. Metals with either excessively strong or weak binding energies exhibit limited N_2 dissociation or slow desorption of N-containing intermediates, leading to a slower catalytic rate.[20] TMs like iron, exhibiting low N_2 dissociation barriers and moderate binding energies, demonstrate superior performance for nitrogen fixation.[21] Iron's abundance and affordability make it a promising candidate for catalyzing NOR.[11,22] The interaction between the active Fe-site and N_2 through hybridization between the 3d and N 2p orbitals activates N_2 and facilitates subsequent NOR.

Previous research showcased the outstanding NOR electrocatalytic performance of FeS_2−TiO_2@2-MeIm/PPy/GO, prepared by FeS_2−TiO_2 heterogeneous nanoparticles in situ growing on 2-methylimidazolium functionalized polypyrrole/graphene oxide (2-MeIm/PPy/GO). However, its stability remained a concern because FeS_2−TiO_2 heterogeneous nanoparticles can spontaneously convert to Fe doped-TiO_2 nanoparticles during the NOR process confirmed by X-ray diffraction (XRD) and X-ray photoelectron spectroscopy (XPS), resulting in the reconstruction of the catalytic center and thereby significantly reducing the NOR electroactivity.[23] To address this, a novel catalyst, FeOOH−TiO_2@2-MeIm/PPy/GO, was developed by replacing FeS_2 with FeOOH using a similar preparation method. This new material exhibits exceptional electrocatalytic NOR performance, achieving the

https://doi.org/10.1021/acsami.5c16699
ACS Appl. Mater. Interfaces XXXX, XXX, XXX−XXX

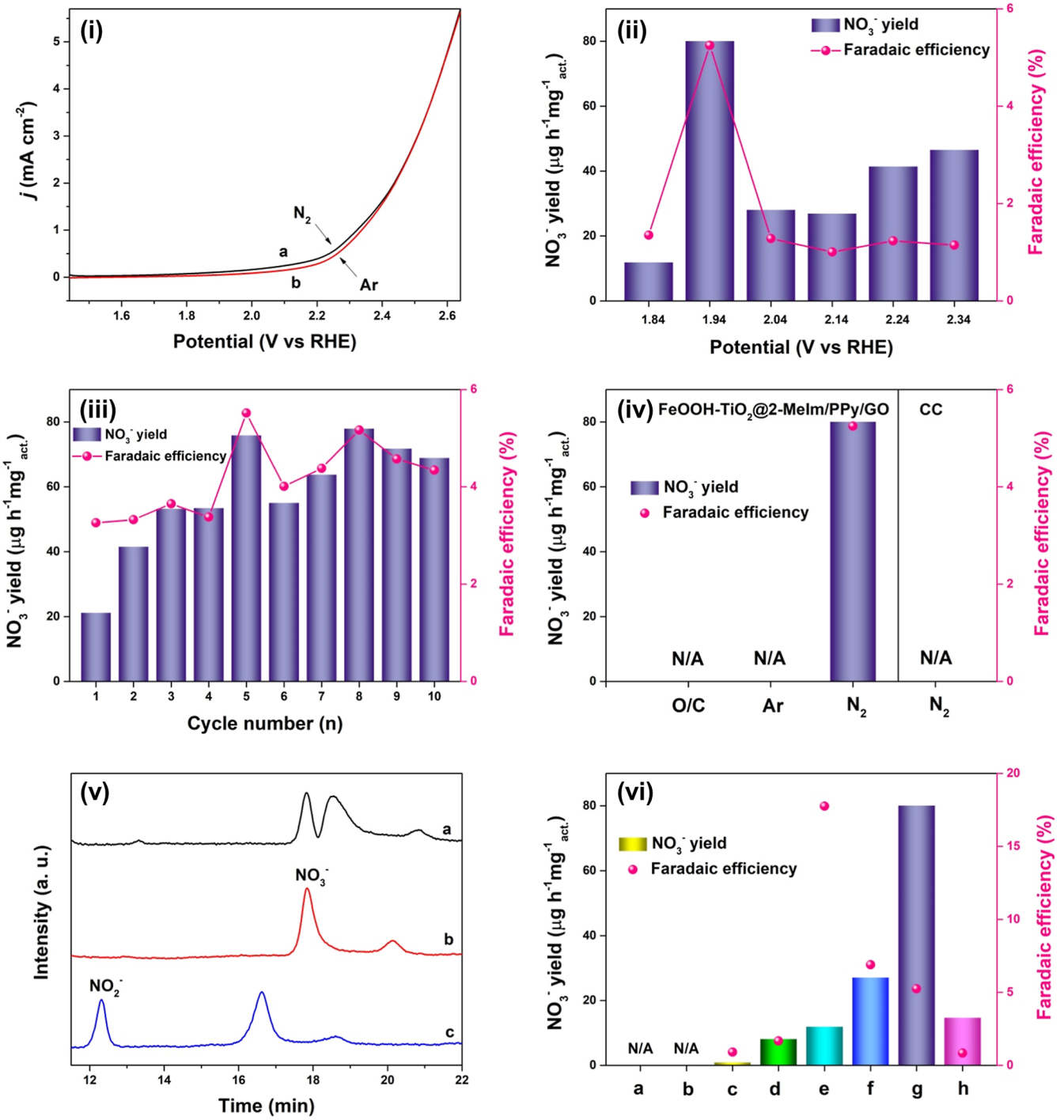

Figure 2. (i) LSV of FeOOH−TiO_2@2-MeIm/PPy/GO under saturated Ar and N_2 in 0.1 M KOH; (ii) the NO_3^- yield and FE of FeOOH−TiO_2@2-MeIm/PPy/GO for NOR at different potentials (vs RHE); (iii) recycling test for FeOOH−TiO_2@2-MeIm/PPy/GO at 1.94 V (vs RHE) under electrolysis for 2 h performed ten times; (iv) the electroactivity of CC (substrate) and FeOOH−TiO_2@2-MeIm/PPy/GO toward NOR at 1.94 V under different conditions; (v) ion chromatogram spectra of (a) the diluted electrolyte after NOR by FeOOH−TiO_2@2-MeIm/PPy/GO at 1.94 V(vs RHE), (b) the standard NO_3^- of 0.2 μg mL^{-1}, (c) the standard NO_2^- of 0.2 μg mL^{-1}; (vi) the NO_3^- yield and FE obtained by different electrocatalysts at 1.94 V(vs RHE) under electrolysis for 2 h: (a) GO, (b) PPy/GO, (c) 2-MeIm/PPy/GO, (d) FeOOH−TiO_2, (e) FeOOH−TiO_2@GO, (f) FeOOH−TiO_2@PPy/GO, (g) FeOOH−TiO_2@2-MeIm/PPy/GO, and (h) TiO_2@2-MeIm/PPy/GO.

highest NO_3^- yield of 83.24 μg h^{-1} $mg_{cat.}^{-1}$ and the maximum FE is 5.47% at 1.94 V (vs reversible hydrogen electrode (RHE)), while simultaneously demonstrating improved stability for NOR. XPS analysis reveals that TiO_2 in FeOOH−TiO_2@2-MeIm/PPy/GO is doped with both Fe^{2+} and Ti^{3+} ions, indicating a synergistic effect between Fe and Ti. Notably, a few Ti^{3+} ions remain stabilized around Ti^{4+}, likely resulting from the conversion of Ti^{4+} reduced by Fe^{2+} during the preparation process. The NOR process primarily occurs at Fe sites, which gradually oxidize to Fe^{3+} during the reaction. Conversely, Ti-sites in FeOOH−TiO_2@2-MeIm/PPy/GO maintain a stable chemical state, providing efficient oxygen

https://doi.org/10.1021/acsami.5c16699
ACS Appl. Mater. Interfaces XXXX, XXX, XXX−XXX

evolution reaction (OER) electroactivity to generate *O for the nonelectrochemical step of NOR. This contributes to the enhanced stability and durability of FeOOH−TiO_2@2-MeIm/PPy/GO toward NOR. This study provides valuable insights into designing and preparing stable and efficient NOR electrocatalysts, paving the way for practical applications in sustainable chemical processes.

2. EXPERIMENTAL SECTION

2.1. Preparation of FeOOH−TiO_2@2-MeIm/PPy/GO Nanosheets. First, presynthesized 2-MeIm/PPy/GO was dispersed in 30 mL of ultrapure water using ultrasound for 15 min. Simultaneously, a solution containing K_2TiF_6 (24 mg), $FeCl_2{\cdot}4H_2O$ (5 mg), and urea (60 mg) was prepared in another 20 mL of ultrapure water, maintaining a Fe/Ti molar ratio of 1/4. The two solutions were then combined under magnetic agitation for 5 min. This mixture was transferred to a sealed 100 mL Teflon-lined stainless steel autoclave and heated at 200 °C for 24 h. After cooling, the resulting black powder was collected via centrifugation by using ethanol and water washes. Finally, it was dried under a vacuum at 50 °C for 24 h.

To investigate the influence of individual components, alternative electrocatalysts such as FeOOH−TiO_2, FeOOH−TiO_2@GO, and FeOOH−TiO_2@PPy/GO were synthesized by using identical reaction parameters. The electrocatalytic performance of these materials for NOR was subsequently evaluated and compared under consistent experimental conditions. The used chemical reagents, characterizations, and apparatus are shown in the Supporting Information in detail.

2.2. Preparation of FeOOH−TiO_2@2-MeIm/PPy/GO Nanosheets Coated on Carbon Cloth. The FeOOH−TiO_2@2-MeIm/PPy/GO suspension was prepared by adding 4 mg of FeOOH−TiO_2@2-MeIm/PPy/GO nanosheets into 920 μL of ethanol mixed with 80 μL of Nafion perfluorinated resin solution, and ultrasound dispersed evenly for 30 min. A working electrode was constructed by dropping the above catalyst suspension onto a carbon cloth (CC) with an area of 1.0 cm × 1.0 cm, used for conducting chronoamperometric measurements. The mass of FeOOH−TiO_2@2-MeIm/PPy/GO coated on CC was calculated by weighing after drying at 50 °C for 12 h.

2.3. Electrochemical Measurements. The electrochemical performance of FeOOH−TiO_2@2-MeIm/PPy/GO was investigated by chronoamperometry with a CHI1040C Electrochemical Station (Shanghai CHENHUA Instrument Co., Ltd.). All the measurements were performed in 0.1 M KOH (pH 12.6) containing saturated Ar or N_2 at room temperature. The chronoamperometry tests for detecting NO_3^- were performed in 50 mL of 0.1 M KOH solution in a standard three-electrode system using FeOOH−TiO_2@2-MeIm/PPy/GO coated on CC as the working electrode, a platinum plate as the counter electrode, and a Ag/AgCl electrode as the reference electrode. The measured potentials versus Ag/AgCl Ag/AgCl were converted to reversible hydrogen electrode (RHE) scale according to the Nernst equation ($E_{RHE} = E_{Ag/AgCl} + 0.059pH + 0.197$). The standard curves and the calculation processes are shown in the Supporting Information in detail.

3. RESULTS AND DISCUSSION

Figure 1 unveils the intricate morphology and crystal structure of FeOOH−TiO_2@2-MeIm/PPy/GO through powerful microscopy techniques. Scanning electron microscopy (SEM) and high-resolution transmission electron microscopy (HRTEM), as shown in Figure 1a,b, reveal a hierarchical marvel: interconnected micro- and nanostructures composed of nanoparticles gracefully interwoven with coiled sheets. After particle size analysis from Figure 1a, the size mean of FeOOH−TiO_2 on 2-MeIm/PPy/GO is around 83 nm. HRTEM analysis, depicted in Figure 1c, delves deeper into the crystal composition. The measured lattice distances of 0.275 and 0.175 nm correspond to the (400) plane of orthorhombic FeOOH and the (105) plane of anatase TiO_2, respectively, confirming their presence within the composite. XRD further solidifies these findings. Figure 1d displays distinct diffraction peaks aligned with JCPDS files for both anatase TiO_2 and orthorhombic FeOOH. Notably, ICP analysis reveals a mass ratio of approximately 9.52% FeOOH to 30.80% TiO_2, as detailed in Table S1.

To gauge the catalytic prowess of FeOOH−TiO_2@2-MeIm/PPy/GO, we immersed it in an H-type electrolytic cell separated with a Nafion membrane and filled with a 0.1 M KOH solution and compared its performance against several control samples: FeOOH−TiO_2@PPy/GO, FeOOH−TiO_2@GO, FeOOH−TiO_2, 2-MeIm/PPy/GO, PPy/GO, and GO. The linear scanning voltammetry (LSV) curve for FeOOH−TiO_2@2-MeIm/PPy/GO, presented in Figure 2i, reveals a heightened current density under a N_2 atmosphere at elevated potentials compared to an Ar atmosphere. This compelling observation clearly demonstrates the electrocatalytic NOR activity of FeOOH−TiO_2@2-MeIm/PPy/GO. Chronoamperometry (CA) experiments, conducted over 2 h at a voltage range of 1.84 to 2.34 V (vs RHE) under N_2 atmosphere, were crucial in assessing the NOR efficiency. The concentrations of NO_3^- and NO_2^- were calculated by the calibration curve in Figures S1 and S2. The results, illustrated in Figure 2ii, pinpoint the optimal potential for NOR as 1.94 V (vs RHE), achieving an impressive peak NO_3^- production rate of 83.24 $\mu g\ h^{-1}\ mg_{act.}^{-1}$, coupled with a maximum FE of 5.47%. This significantly surpasses the performance observed at other voltages. Finally, we evaluated the catalytic stability of FeOOH−TiO_2@2-MeIm/PPy/GO over 10 cycles at an optimal voltage for 2 h per cycle. As shown in Figure 2iii, both the NO_3^- yield and FE initially surged during the first five cycles, peaking in cycle five before a gradual decline. However, even by cycle ten, a substantial NO_3^- yield of 68.95 $\mu g\ h^{-1}\ mg_{act.}^{-1}$ was maintained, showcasing remarkable stability for FeOOH−TiO_2@2-MeIm/PPy/GO in this demanding NOR process. Obviously, the NOR performance of FeOOH−TiO_2@2-MeIm/PPy/GO is better than most of most previously reported NOR electrocatalysts based on non-noble metals in Table S2, especially the improved outstanding stability compared to electrocatalysts based on TiO_2, including Ru/TiO_2,[5] Pd/S−TiO_2@2-MeIm/PPy/GO[7], and FeS_2−TiO_2@2-MeIm/PPy/GO.[23]

To unravel the fascinating origins of nitrogen within the produced nitrate and pinpoint the remarkable selectivity of FeOOH−TiO_2@2-MeIm/PPy/GO, a series of meticulous experiments were conducted. As depicted in Figure 2iv, FeOOH−TiO_2@2-MeIm/PPy/GO remained stubbornly silent under both an Ar-saturated electrolyte at 1.94 V (vs RHE) and open circuit conditions within a nitrogen-saturated electrolyte. Furthermore, no nitrate was yielded by employing CC as the electrocatalyst in the N_2-saturated electrolyte, which is a compelling testament that the nitrogen found in NO_3^- originated solely from the electrocatalytic oxidation of N_2 present within the gas feedstock. A captivating comparison of ion chromatographic profiles further solidified the exceptional selectivity of FeOOH−TiO_2@2-MeIm/PPy/GO. Comparing the ion chromatographic profiles of standard 0.3 $\mu g\ mL^{-1}$ of NO_3^- and NO_2^- (Figure 2v(b,c)), a prominent peak corresponding to NO_3^- appeared in Figure 2v(a), while no trace of NO_2^- is detected. This absence of byproducts underscores the remarkable precision with which FeOOH−

https://doi.org/10.1021/acsami.5c16699
ACS Appl. Mater. Interfaces XXXX, XXX, XXX−XXX

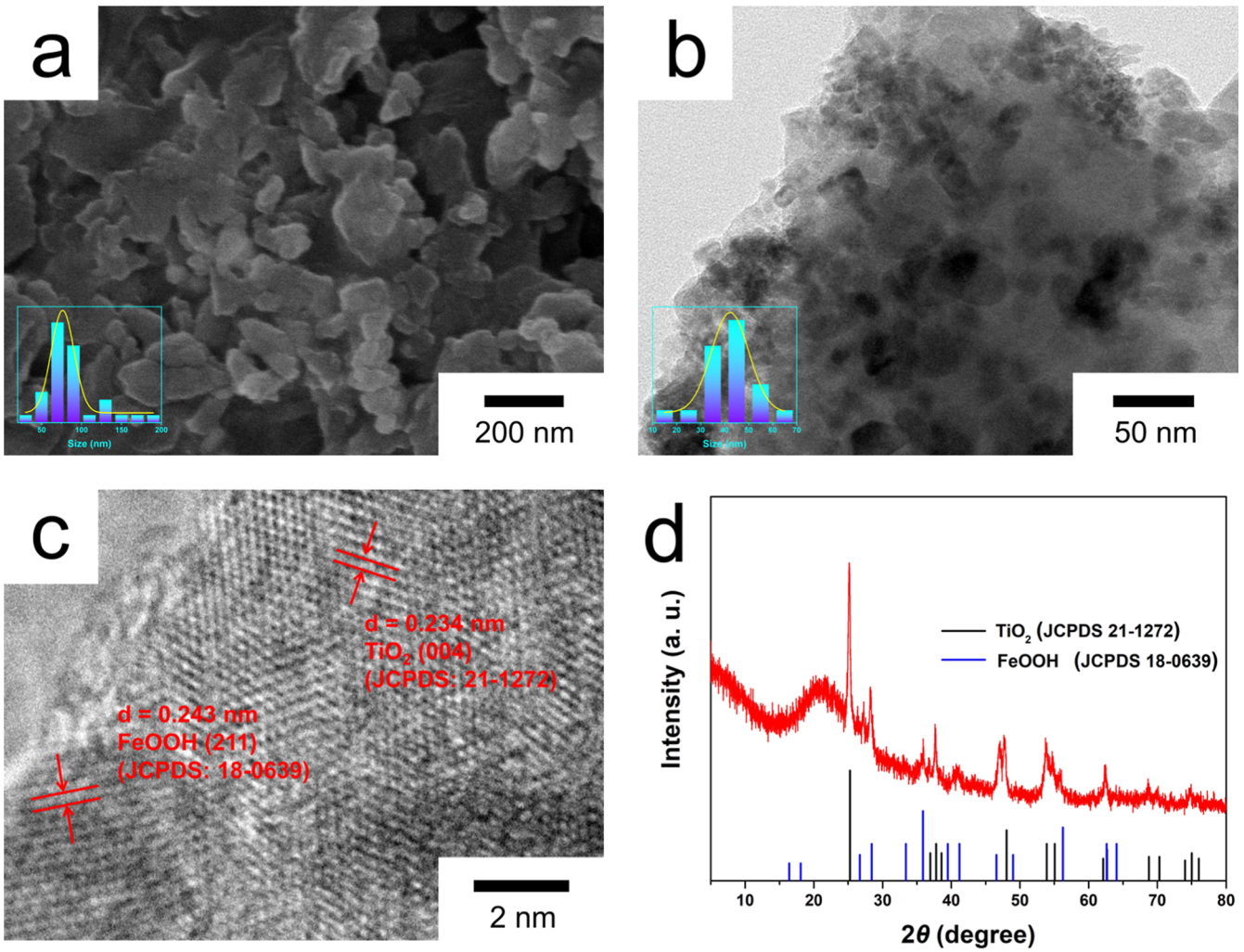

Figure 3. (a) SEM image; (b) TEM image; (c) HRTEM image; (d) XRD pattern of FeOOH−TiO_2@2-MeIm/PPy/GO after electrolysis for 30 h in N_2 saturated electrolyte.

TiO_2@2-MeIm/PPy/GO orchestrates nitrate production via electrocatalytic NOR. Figure 2vi presents a panoramic view of the NOR electroactivity across various catalysts synthesized with different supports. A sobering reality emerges: all supporters pale in comparison to FeOOH−TiO_2, highlighting the pivotal role it plays in this process. However, the inherent tendency of FeOOH−TiO_2 nanoparticles to aggregate (as depicted in Figure S3a) restricts their performance, yielding a modest 8.12 μg h^{-1} $mg_{act.}^{-1}$ with an FE of 1.67% at 1.94 V (vs RHE). When compared to the morphologies of FeOOH−TiO_2@GO and FeOOH−TiO_2@PPy/GO (as depicted in Figure S3b,c), the dispersion of FeOOH−TiO_2 nanoparticles on the surface of 2-MeIm/PPy/GO is significantly improved (as shown in Figure 1a,b). This improvement is attributable to uniform adsorption patterns exhibited by TiF_6^{2-} and Fe^{2+} precursors through ion exchange interactions alongside coordination with functional groups from 2-MeIm. This meticulous arrangement ensures better exposure of active sites, propelling the NOR process forward. While XRD results presented in Figures S3d and 1d confirm consistent phase compositions for FeOOH−TiO_2 across different supports, variations in weight content related to surface loading hold significant sway, as detailed further within Table S1. This subtle yet profound influence on the morphology and catalytic active center content, driven by the support materials, ultimately dictates their electrocatalytic NOR performances. The findings unequivocally demonstrate that 2-MeIm groups can act as masterful architects, enhancing dispersion characteristics for FeOOH−TiO_2, leading to a symphony of enhanced electroactivity during NOR processes. Compared to the subdued NOR electroactivity of TiO_2@2-MeIm/PPy/GO with the NO_3^- yield of 14.69 μg h^{-1} $mg_{act.}^{-1}$ and a corresponding FE of 0.84% at 1.94 V (vs RHE), the NOR process on FeOOH−TiO_2@2-MeIm/PPy/GO flourishes primarily at Fe-sites, while Ti-sites diligently engage in OER, which is an invaluable contribution that further provides *O for the nonelectrochemical step of NOR, propelling nitrate generation to new heights.

To further characterize the NOR process on FeOOH−TiO_2@2-MeIm/PPy/GO, the sample's morphology, phase composition, and chemical state were analyzed using SEM, HRTEM, XRD, and XPS after extended electrolysis in a N_2-saturated electrolyte. As shown in Figure 3a,b, the NOR-processed FeOOH−TiO_2@2-MeIm/PPy/GO retains its hierarchical micro/nanostructures, comprising nanoparticles and curly sheets, with no significant morphological or structural changes compared to the as-synthesized sample. The particle size of FeOOH−TiO_2 on 2-Melm/PPy/GO has barely

https://doi.org/10.1021/acsami.5c16699
ACS Appl. Mater. Interfaces XXXX, XXX, XXX−XXX

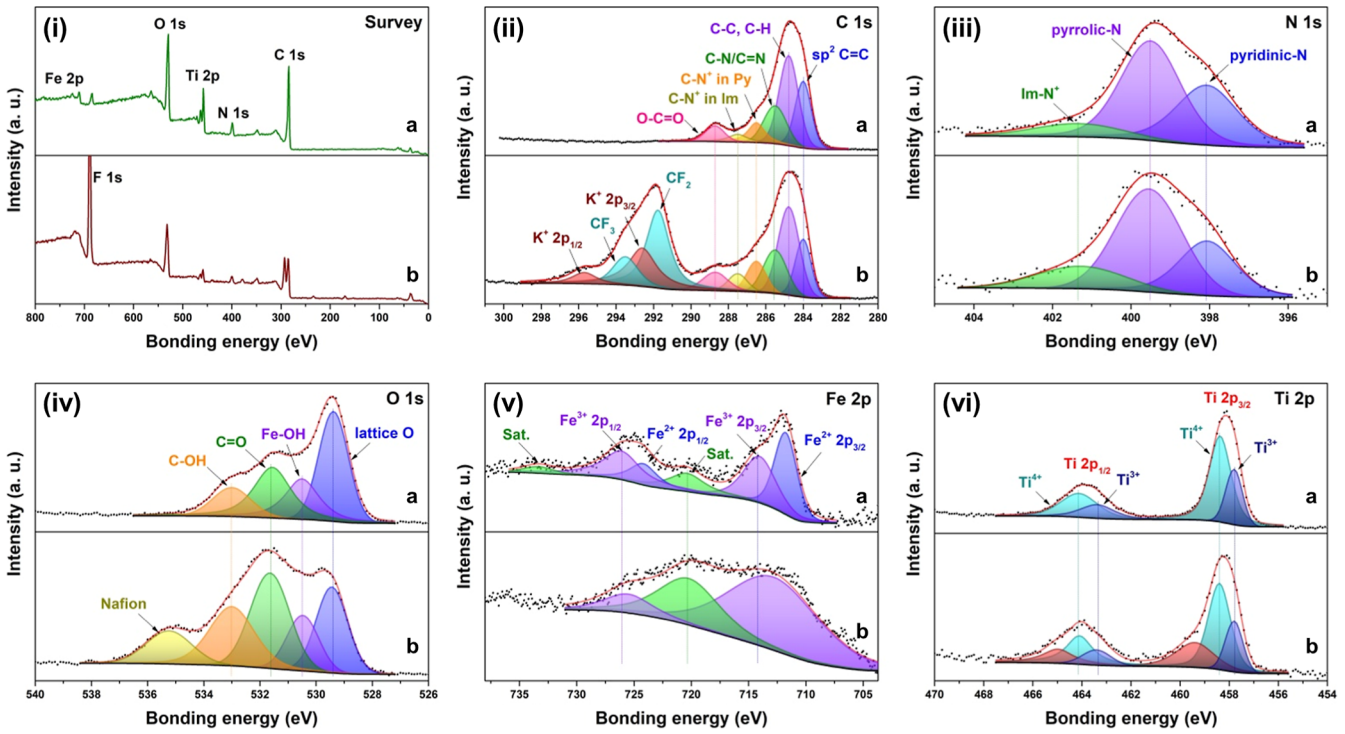

Figure 4. XPS spectra of FeOOH−TiO_2@2-MeIm/PPy/GO (a) before and (b) after electrolysis for 30 h in N_2 saturated electrolyte: (i) survey; (ii) C 1s; (iii) N 1s; (iv) O 1s; (v) Fe 2p; and (vi) Ti 2p.

changed, whose size mean is still around 83 nm due to the particle size analysis from Figure 3a. The HRTEM image in Figure 3c demonstrates lattice spacings of 0.234 and 0.243 nm for FeOOH−TiO_2@2-MeIm/PPy/GO post-NOR treatment, which correspond to TiO_2 (004) and FeOOH (211) lattice spacings, respectively. Additionally, the XRD pattern in Figure 3d confirms that the diffraction peaks of FeOOH−TiO_2@2-MeIm/PPy/GO after prolonged electrolysis closely match those of anatase TiO_2 (JCPDS No. 21-1272) and orthorhombic FeOOH (JCPDS No. 18-0639). In addition, the decay rate of the NO_3^- yield of a single continuous electrolysis for 24 h is calculated to be 21.56%. These results collectively indicate that FeOOH−TiO_2@2-MeIm/PPy/GO exhibits remarkable chemical stability during the NOR process, contributing to its excellent cycling stability and durability.

The chemical state of FeOOH−TiO_2@2-MeIm/PPy/GO before and after long-term NOR process was well confirmed by XPS in Figure 4. The peaks of C 1s, N 1s, O 1s, Fe 2p, and Ti 2p can be clearly observed in the survey spectra of FeOOH−TiO_2@2-MeIm/PPy/GO before and after NOR (Figure 4i(a)), and F 1s peak appears in Figure 4i(b) due to the added Nafion perfluorinated resin. For C 1s spectra, six peaks at 284.0, 284.8, 285.5, 286.5, 287.5, and 288.7 eV in Figure 4ii(a) are attributed to sp^2 C═C,[24] C−C/C−H,[25] C−N/C═N in pyrrole ring,[26] C−N^+ in pyrrole ring,[27] C−N^+ in imidazolium ring,[28] and O−C═O group,[29] respectively. Meanwhile, four additional peaks at 291.8, 292.6, 293.5, and 295.7 eV in Figure 4ii(b) are associated with −CF_2- group,[30] K^+ $2p_{3/2}$,[31] −CF_3 group,[32] and K^+ $2p_{1/2}$,[33] respectively, caused by the adsorbed KOH and the added Nafion perfluorinated resin. Three peaks located at 398.1, 399.5, and 401.3 eV in N 1s spectra of FeOOH−TiO_2@2-MeIm/PPy/GO before and after NOR (Figure 4iii) belong to pyridinic-N,[34] pyrrolic-N,[35] and N^+ in the imidazolium ring,[36] respectively, well confirming the presence of the imidazolium ion on the surface of PPy/GO. For O 1s region, an additional peak at 535.2 eV in Figure 4iv(b) indicates the presence of etheric groups in Nafion and other four peaks are assigned to lattice O (529.4 eV),[37] Fe−OH (530.5 eV),[38] C═O (531.6 eV),[39] and C−OH (533.0 eV),[40] respectively. The Fe 2p core-line spectra of FeOOH−TiO_2@2-MeIm/PPy/GO before NOR can be fitted with six peaks in Figure 4v(a), ascribed to Fe^{2+} $2p_{3/2}$ (710.5 eV),[41] Fe^{3+} $2p_{3/2}$ (712.8 eV),[41] satellite peak (719.5 eV),[42] Fe^{2+} $2p_{1/2}$ (723.5 eV),[41] Fe^{3+} $2p_{1/2}$ (725.5 eV),[41] and satellite peak (733.1 eV),[43] respectively, where Fe^{2+} may exist in TiO_2 in doped form and Fe^{3+} exist in FeOOH. But post-NOR treatment, only three peaks remain and correspond to Fe^{3+} $2p_{3/2}$, satellite peak, and Fe^{3+} $2p_{1/2}$, indicating the oxidation of all Fe^{2+} to Fe^{3+}. In the Ti 2p spectra (Figure 4vi), when the electrocatalysts were synthesized, two pairs of peaks were fitted in Figure 4vi(a). A pair of peaks located at 457.8 and 463.4 eV are corresponding to Ti^{3+} $2p_{3/2}$ and Ti^{3+} $2p_{1/2}$ orbits,[44] derived from the conversion of Ti^{4+} to Ti^{3+} reduced by Fe^{2+} during the prepared process, while another pair of peaks located at 458.4 and 464.1 eV are corresponding to Ti^{4+} $2p_{3/2}$ and Ti^{4+} $2p_{1/2}$ orbits,[45] respectively. The ratio of Ti^{3+} to Ti^{4+} is approximately calculated to 1:2.48. According to the data analysis results of Fe 2p and Ti 2p spectra of FeOOH−TiO_2@2-MeIm/PPy/GO as synthesized, TiO_2 may be doped by Fe^{2+} and Ti^{3+}. After NOR, these two pairs of peaks also appear in Figure 4vi(b). The ratio of Ti^{3+} to Ti^{4+} is approximately calculated to 1:2.51, which is much close to the ratio of Ti^{3+} to Ti^{4+} for the as-synthesized electrocatalysts, indicating that TiO_2 exhibits excellent chemical stability during the NOR process. However, a small pair of peaks appear at 459.4 and 465.0 eV, indicating a shift of Ti^{4+} $2p_{3/2}$ and Ti^{4+} $2p_{1/2}$ orbits of anatase TiO_2 to higher binding energy, which may be due to an increase in the positive charge of the transition metal atoms[46] caused by

https://doi.org/10.1021/acsami.5c16699
ACS Appl. Mater. Interfaces XXXX, XXX, XXX−XXX

electrochemical power source. The analysis of Fe 2p and Ti 2p spectra suggests that most of the Fe and Ti remain in their stable chemical states post-NOR and that a few Ti^{3+} ions are well stabilized around Ti^{4+}. As reported, Fe exhibits superior nitrogen activation capabilities compared to Ti,[47] indicating lower N_2 dissociation barriers and moderate binding energies, which contribute to its superior electrocatalytic performance for nitrogen fixation.[21,23] Therefore, the NOR process may dominantly occur at the Fe-sites, which are gradually oxidized to Fe^{3+} during the NOR process, while Ti-sites in FeOOH−TiO_2@2-MeIm/PPy/GO are always in a stable chemical state, providing appropriate OER electroactivity to generate *O for the nonelectrochemical step of NOR, resulting in the good stability and durability of FeOOH−TiO_2@2-MeIm/PPy/GO toward NOR.

4. CONCLUSIONS

In summary, the well-dispersed FeOOH−TiO_2 heterostructures were grown in situ on the surface of 2-MeIm/PPy/GO due to ion exchange and coordination between 2-MeIm and metal precursors. The resulting FeOOH−TiO_2@2-MeIm/PPy/GO exhibited an excellent NOR electrocatalytic performance and selectivity for nitrate generation. The catalyst achieved the highest NO_3^- yield of 83.24 $\mu g\ h^{-1}\ mg_{act.}^{-1}$ at 1.94 V (vs RHE) with a maximum Faradaic efficiency of 5.47%. Cyclic experiments demonstrated that the NO_3^- yield and Faradaic efficiency of FeOOH−TiO_2@2-MeIm/PPy/GO gradually increased in the initial cycles, peaked in the eighth cycle, and then maintained stability with a slight decline. By comprehensive comparison including the morphology, phase composition, and chemical state of FeOOH−TiO_2@2-MeIm/PPy/GO before and after long-term NOR process, it is speculated that the NOR reaction primarily occurred at Fe sites, and the doped Fe^{2+} in TiO_2 can all gradually transition to Fe^{3+} throughout the process. Conversely, Ti sites maintained stable chemical states, ensuring sufficient electroactivity for the OER, which was a crucial step in producing *O* required for essential nonelectrochemical steps in NOR. This synergistic interplay between Fe and Ti contributed significantly to both the stability and durability of FeOOH−TiO_2@2-MeIm/PPy/GO, positioning it as a promising candidate for real-world NOR applications.

■ ASSOCIATED CONTENT

Supporting Information

The Supporting Information is available free of charge at https://pubs.acs.org/doi/10.1021/acsami.5c16699.

Materials; preparation of 2-MeIm/PPy/GO nanosheets; preparation of TiO_2@2-MeIm/PPy/GO; preparation of FeOOH−TiO_2@2-MeIm/PPy/GO nanosheets modified GCE; characterizations and apparatus; nitrate detection; nitrite detection; computational formula; calibration curves; and SEM images and tables (PDF)

■ AUTHOR INFORMATION

Corresponding Authors

Rui Zhang − *Shenyang Key Laboratory of Medical Molecular Theranostic Probes in School of Pharmacy, School of Pharmacy, Shenyang Medical College, Shenyang 110034, P. R. China*; Email: ruizhang@symc.edu.cn

Daliang Liu − *Institute of Clean Energy Chemistry, Key Laboratory for Green Synthesis and Preparative Chemistry of Advanced Materials, College of Chemistry, Liaoning University, Shenyang 110036, P. R. China*; Email: dalianglliu@lnu.edu.cn

Hui Mao − *Institute of Clean Energy Chemistry, Key Laboratory for Green Synthesis and Preparative Chemistry of Advanced Materials, College of Chemistry, Liaoning University, Shenyang 110036, P. R. China*; orcid.org/0000-0002-1898-2474; Email: huimao@lnu.edu.cn

Authors

Huinan Li − *Institute of Clean Energy Chemistry, Key Laboratory for Green Synthesis and Preparative Chemistry of Advanced Materials, College of Chemistry, Liaoning University, Shenyang 110036, P. R. China*

Yuheng Sun − *Institute of Clean Energy Chemistry, Key Laboratory for Green Synthesis and Preparative Chemistry of Advanced Materials, College of Chemistry, Liaoning University, Shenyang 110036, P. R. China*

Shuyao Wu − *Institute of Clean Energy Chemistry, Key Laboratory for Green Synthesis and Preparative Chemistry of Advanced Materials, College of Chemistry, Liaoning University, Shenyang 110036, P. R. China*

Qiong Wu − *Institute of Clean Energy Chemistry, Key Laboratory for Green Synthesis and Preparative Chemistry of Advanced Materials, College of Chemistry, Liaoning University, Shenyang 110036, P. R. China*

Tianyi Ma − *Centre for Atomaterials and Nanomanufacturing (CAN), School of Science, RMIT University, Melbourne, Victoria 3000, Australia; ARC Industrial Transformation Research Hub for Intelligent Energy Efficiency in Future Protected Cropping (E2Crop), Melbourne, Victoria 3000, Australia*; orcid.org/0000-0002-1042-8700

Complete contact information is available at: https://pubs.acs.org/10.1021/acsami.5c16699

Author Contributions

[⊥]R.Z. and H.L. contributed equally to this paper.

Notes

The authors declare no competing financial interest.

■ ACKNOWLEDGMENTS

R.Z. thanked the Foundation of Liaoning Province Education Administration (2020LQN03), the Foundation of Liaoning Province Education Administration in 2024 (Independent topic selection-Natural science category-Strategic industrialization project LJ212410163023), and the Natural Science Foundation of Liaoning Province (2025-MS-295). H.M. thanked the Liaoning Revitalization Talents Program (XLYC2007132). T.M. acknowledged the Australian Research Council (ARC) through Future Fellowship (FT210100298), Discovery Project (DP220100603), Linkage Project (LP210200504, LP220100088, LP230200897), and Industrial Transformation Research Hub (IH240100009) schemes, the Australian Government through the Cooperative Research Centres Projects (CRCPXIII000077), the Australian Renewable Energy Agency (ARENA) as part of ARENA's Transformative Research Accelerating Commercialisation Program (TM021), and European Commission's Australia-Spain Network for Innovation and Research Excellence (AuSpire). The authors would like to thank Yao Fan and Gao Jilong from Shiyanjia Lab (www.shiyanjia.com) for the XPS and ICP analysis.

https://doi.org/10.1021/acsami.5c16699
ACS Appl. Mater. Interfaces XXXX, XXX, XXX−XXX

REFERENCES

(1) Tang, C.; Zheng, Y.; Jaroniec, M.; Qiao, S. Z. Electrocatalytic refinery for sustainable production of fuels and chemicals. *Angew. Chem., Int. Ed.* **2021**, *60* (36), 19572−19590.

(2) Sharif, H. M. A.; Khan, H. M. F.; Ullah, S.; Wang, Y.; Ahmad, M.; Yang, B.; Li, C.; Asif, M. B. Progress in electrocatalytic nitrate reduction for green energy: Catalyst engineering, mechanisms, and techno-economic feasibility. *J. Energy Chem.* **2024**, *95*, 380−406.

(3) Centi, G.; Perathoner, S. Status and gaps toward fossil-free sustainable chemical production. *Green Chem.* **2022**, *24* (19), 7305−7331.

(4) Xia, P.; Pan, X.; Jiang, S.; Yu, J.; He, B.; Ismail, P. M.; Bai, W.; Yang, J.; Yang, L.; Zhang, H.; et al. Designing a redox heterojunction for photocatalytic "overall nitrogen fixation" under mild conditions. *Adv. Mater.* **2022**, *34* (28), 2200563.

(5) Kuang, M.; Wang, Y.; Fang, W.; Tan, H.; Chen, M.; Yao, J.; Liu, C.; Xu, J.; Zhou, K.; Yan, Q. Efficient nitrate synthesis via ambient nitrogen oxidation with Ru-doped TiO_2/RuO_2 electrocatalysts. *Adv. Mater.* **2020**, *32* (26), 2002189.

(6) Han, S.; Wang, C.; Wang, Y.; Yu, Y.; Zhang, B. Electrosynthesis of Nitrate via the Oxidation of Nitrogen on Tensile-Strained Palladium Porous Nanosheets. *Angew. Chem.* **2021**, *133* (9), 4524−4528.

(7) Mao, H.; Sun, Y.; Li, H.; Wu, S.; Liu, D.; Li, H.; Li, S.; Ma, T. Synergy of Pd^{2+}/S^{2-} Doped TiO_2 Supported on 2-methylimidazolium Functionalized Polypyrrole/Graphene Oxide for Enhanced Nitrogen Electro-Oxidation. *Adv. Mater.* **2024**, *36* (16), 2313155.

(8) Qiu, W.; Xie, X.-Y.; Qiu, J.; Fang, W.-H.; Liang, R.; Ren, X.; Ji, X.; Cui, G.; Asiri, A. M.; Cui, G.; et al. High-performance artificial nitrogen fixation at ambient conditions using a metal-free electrocatalyst. *Nat. Commun.* **2018**, *9* (1), 3485.

(9) Yang, C.; Zhu, Y.; Liu, J.; Qin, Y.; Wang, H.; Liu, H.; Chen, Y.; Zhang, Z.; Hu, W. Defect engineering for electrochemical nitrogen reduction reaction to ammonia. *Nano Energy* **2020**, *77*, 105126.

(10) Liu, D.; Chen, M.; Du, X.; Ai, H.; Lo, K. H.; Wang, S.; Chen, S.; Xing, G.; Wang, X.; Pan, H. Development of electrocatalysts for efficient nitrogen reduction reaction under ambient condition. *Adv. Funct. Mater.* **2021**, *31* (11), 2008983.

(11) Zhang, L.; Cong, M.; Ding, X.; Jin, Y.; Xu, F.; Wang, Y.; Chen, L.; Zhang, L. A janus Fe-SnO_2 catalyst that enables bifunctional electrochemical nitrogen fixation. *Angew. Chem.* **2020**, *132* (27), 10980−10985.

(12) Dai, C.; Sun, Y.; Chen, G.; Fisher, A. C.; Xu, Z. J. Electrochemical oxidation of nitrogen towards direct nitrate production on spinel oxides. *Angew. Chem., Int. Ed.* **2020**, *59* (24), 9418−9422.

(13) Nie, Z.; Zhang, L.; Ding, X.; Cong, M.; Xu, F.; Ma, L.; Guo, M.; Li, M.; Zhang, L. Catalytic Kinetics Regulation for Enhanced Electrochemical Nitrogen Oxidation by Ru-Nanoclusters-Coupled Mn3O4 Catalysts Decorated with Atomically Dispersed Ru Atoms. *Adv. Mater.* **2022**, *34* (14), 2108180.

(14) Li, J.; Li, Z.; Sun, Q.; Wang, Y.; Li, Y.; Peng, Y. K.; Li, Y.; Zhang, C.; Liu, B.; Zhao, Y. Recent Advances in the Large-Scale Production of Photo/Electrocatalysts for Energy Conversion and beyond. *Adv. Energy Mater.* **2024**, *14* (45), 2402441.

(15) Sui, X.; Zhang, L.; Li, J.; Doyle-Davis, K.; Li, R.; Wang, Z.; Sun, X. Advanced support materials and interactions for atomically dispersed noble-metal catalysts: from support effects to design strategies. *Adv. Energy Mater.* **2022**, *12* (1), 2102556.

(16) Antolini, E. Structural parameters of supported fuel cell catalysts: The effect of particle size, inter-particle distance and metal loading on catalytic activity and fuel cell performance. *Appl. Catal., B* **2016**, *181*, 298−313.

(17) Lü, F.; Zhao, S.; Guo, R.; He, J.; Peng, X.; Bao, H.; Fu, J.; Han, L.; Qi, G.; Luo, J.; et al. Nitrogen-coordinated single Fe sites for efficient electrocatalytic N2 fixation in neutral media. *Nano Energy* **2019**, *61*, 420−427.

(18) Yang, Q.; Guo, Y.; Gu, J.; Li, N.; Wang, C.; Liu, Z.; Li, X.; Huang, Z.; Wei, S.; Xu, S.; et al. Scalable synthesis of 2D hydrogen-substituted graphdiyne on Zn substrate for high-yield N_2 fixation. *Nano Energy* **2020**, *78*, 105283.

(19) Rösch, B.; Gentner, T.; Langer, J.; Färber, C.; Eyselein, J.; Zhao, L.; Ding, C.; Frenking, G.; Harder, S. Dinitrogen complexation and reduction at low-valent calcium. *Science* **2021**, *371* (6534), 1125−1128.

(20) Jacobsen, C. J.; Dahl, S.; Clausen, B. S.; Bahn, S.; Logadottir, A.; Nørskov, J. K. Catalyst design by interpolation in the periodic table: bimetallic ammonia synthesis catalysts. *J. Am. Chem. Soc.* **2001**, *123* (34), 8404−8405.

(21) Li, Y.; Li, Y.; Wang, B.; Luo, Y.; Yang, D.; Tong, P.; Zhao, J.; Luo, L.; Zhou, Y.; Chen, S.; et al. Ammonia formation by a thiolate-bridged diiron amide complex as a nitrogenase mimic. *Nat. Chem.* **2013**, *5* (4), 320−326.

(22) Guo, Y.; Zhang, S.; Zhang, R.; Wang, D.; Zhu, D.; Wang, X.; Xiao, D.; Li, N.; Zhao, Y.; Huang, Z.; et al. Electrochemical nitrate production via nitrogen oxidation with atomically dispersed Fe on N-doped carbon nanosheets. *ACS Nano* **2021**, *16* (1), 655−663.

(23) Mao, H.; Li, H.; Sun, Y.; Wu, S.; Wu, Q.; Liu, D.; Ma, T. Electrosynthesis of nitrate by FeS_2-TiO_2 heterogeneous nanoparticles supported on 2-methylimidazolium functionalized polypyrrole/graphene oxide. *Chem. Eng. J.* **2024**, *489*, 151414.

(24) Hu, R.; Furukawa, T.; Wang, X.; Nagatsu, M. Morphological study of graphite-encapsulated iron composite nanoparticles fabricated by a one-step arc discharge method. *Appl. Surf. Sci.* **2017**, *416*, 731−741.

(25) Li, X.; Xue, Z.; Sun, W.; Chu, J.; Wang, Q.; Tong, L.; Wang, K. Bio-inspired self-healing MXene/polyurethane coating with superior active/passive anticorrosion performance for Mg alloy. *Chem. Eng. J.* **2023**, *454*, 140187.

(26) Chen, Y.; Lyu, S.; Han, S.; Chen, Z.; Wang, W.; Wang, S. Nanocellulose/polypyrrole aerogel electrodes with higher conductivity via adding vapor grown nano-carbon fibers as conducting networks for supercapacitor application. *RSC Adv.* **2018**, *8* (70), 39918−39928.

(27) Bharti, M.; Singh, A.; Samanta, S.; Debnath, A.; Aswal, D.; Muthe, K.; Gadkari, S. Flexo-green Polypyrrole−Silver nanocomposite films for thermoelectric power generation. *Energy Convers. Manage.* **2017**, *144*, 143−152.

(28) Pham-Truong, T.-N.; Petenzi, T.; Ranjan, C.; Randriamahazaka, H.; Ghilane, J. Microwave assisted synthesis of carbon dots in ionic liquid as metal free catalyst for highly selective production of hydrogen peroxide. *Carbon* **2018**, *130*, 544−552.

(29) Xiao, D.; Zheng, M.-T.; Wu, F.-J. A bio-inspired self-assembled asymmetrical supramolecular film for highly-sensitive fire warning, solvent response, and smart switching. *Chem. Eng. J.* **2023**, *459*, 141546.

(30) Hamilton, C. E.; Lomeda, J. R.; Sun, Z.; Tour, J. M.; Barron, A. R. Radical addition of perfluorinated alkyl iodides to multi-layered graphene and single-walled carbon nanotubes. *Nano Res.* **2010**, *3*, 138−145.

(31) Yu, G.; Wang, J.; Ma, H.; Liu, X.; Qin, S.; Yang, Z.; Zhang, G.; Li, Y.; Zhu, L. Exploring abundantly synergic effects of K-Cu supported paper catalysts using TiO_2-ZrO_2 mesoporous fibers as matrix towards soot efficient oxidation. *Chem. Eng. J.* **2021**, *417*, 128111.

(32) Cai, Y.; Li, J.; Yi, L.; Yan, X.; Li, J. Fabricating superhydrophobic and oleophobic surface with silica nanoparticles modified by silanes and environment-friendly fluorinated chemicals. *Appl. Surf. Sci.* **2018**, *450*, 102−111.

(33) Che, H.; Wang, J.; Gao, X.; Chen, J.; Wang, P.; Liu, B.; Ao, Y. Regulating directional transfer of electrons on polymeric g-C_3N_5 for highly efficient photocatalytic H_2O_2 production. *J. Colloid Interface Sci.* **2022**, *627*, 739−748.

(34) Zhang, K.; Xu, Y.; Liu, F.; Yan, G.-P.; Guo, S.-W. Preparation and properties of ZnS−CdSe@ Co/N−C core/shell composites for visible light photoconversion of CO_2. *New J. Chem.* **2023**, *47* (27), 12550−12553.

(35) Yuan, T.; He, Y.-S.; Zhang, W.; Ma, Z.-F. A nitrogen-containing carbon film derived from vapor phase polymerized polypyrrole as a

https://doi.org/10.1021/acsami.5c16699
ACS Appl. Mater. Interfaces XXXX, XXX, XXX−XXX

fast charging/discharging capability anode for lithium-ion batteries. *Chem. Commun.* **2016**, *52* (1), 112−115.
(36) Muniandy, L.; Adam, F.; Rahman, N. R. A.; Ng, E.-P. Highly selective synthesis of cyclic carbonates via solvent free cycloaddition of CO_2 and epoxides using ionic liquid grafted on rice husk derived MCM-41. *Inorg. Chem. Commun.* **2019**, *104*, 1−7.
(37) Kim, H. S.; Kim, D.; Kwak, B. S.; Han, G. B.; Um, M.-H.; Kang, M. Synthesis of magnetically separable core@ shell structured $NiFe_2O_4$@TiO_2 nanomaterial and its use for photocatalytic hydrogen production by methanol/water splitting. *Chem. Eng. J.* **2014**, *243*, 272−279.
(38) Wei, B.; Shang, C.; Wang, X.; Zhou, G. Conductive FeOOH as multifunctional interlayer for superior lithium−sulfur batteries. *Small* **2020**, *16* (34), 2002789.
(39) Zhao, J.; Wang, B.; Zhou, Q.; Wang, H.; Li, X.; Chen, H.; Wei, Q.; Wu, D.; Luo, Y.; You, J.; et al. Efficient electrohydrogenation of N_2 to NH_3 by oxidized carbon nanotubes under ambient conditions. *Chem. Commun.* **2019**, *55* (34), 4997−5000.
(40) Xu, M.; Dou, H.; Zhang, Z.; Zheng, Y.; Ren, B.; Ma, Q.; Wen, G.; Luo, D.; Yu, A.; Zhang, L.; et al. Hierarchically Nanostructured Solid-State Electrolyte for Flexible Rechargeable Zinc−Air Batteries. *Angew. Chem.* **2022**, *134* (23), No. e202117703.
(41) Yang, X.; Liping, S.; Qiang, L.; Lihua, H.; Hui, Z. Co-prosperity of electrocatalytic activity and stability in high entropy spinel $(Cr_{0.2}Mn_{0.2}Fe_{0.2}Ni_{0.2}Zn_{0.2})_3O_4$ for the oxygen evolution reaction. *J. Mater. Chem. A* **2022**, *10* (34), 17633−17641.
(42) Liu, J.; Zheng, M.; Shi, X.; Zeng, H.; Xia, H. Amorphous FeOOH quantum dots assembled mesoporous film anchored on graphene nanosheets with superior electrochemical performance for supercapacitors. *Adv. Funct. Mater.* **2016**, *26* (6), 919−930.
(43) Qiu, Y.; Liu, Z.; Zhang, X.; Sun, A.; Liu, J. Synergistic effect of oxidation etching and phase transformation triggered by controllable ion-bath microenvironments toward constructing ultra-thin porous nanosheets for accelerated industrial water splitting at high current density. *J. Colloid Interface Sci.* **2022**, *625*, 50−58.
(44) Zhang, D.; Ma, X.; Zhang, H.; Liao, Y.; Xiang, Q. Enhanced photocatalytic hydrogen evolution activity of carbon and nitrogen self-doped TiO_2 hollow sphere with the creation of oxygen vacancy and Ti^{3+}. *Mater. Today Energy* **2018**, *10*, 132−140.
(45) Tian, L.; Xu, J.; Alnafisah, A.; Wang, R.; Tan, X.; Oyler, N. A.; Liu, L.; Chen, X. A novel green TiO_2 photocatalyst with a surface charge-transfer complex of Ti and hydrazine groups. *Chem.—Eur. J.* **2017**, *23* (22), 5345−5351.
(46) Chetri, P.; Basyach, P.; Choudhury, A. Exploring the structural and magnetic properties of TiO_2/SnO_2 core/shell nanocomposite: An experimental and density functional study. *J. Solid State Chem.* **2014**, *220*, 124−131.
(47) Skulason, E.; Bligaard, T.; Gudmundsdóttir, S.; Studt, F.; Rossmeisl, J.; Abild-Pedersen, F.; Vegge, T.; Jónsson, H.; Nørskov, J. K. A theoretical evaluation of possible transition metal electro-catalysts for N_2 reduction. *Phys. Chem. Chem. Phys.* **2012**, *14* (3), 1235−1245.

https://doi.org/10.1021/acsami.5c16699
ACS Appl. Mater. Interfaces XXXX, XXX, XXX−XXX